Chapter 16

NEGATIVE-MASS INSTABILITY

Near transition, the slippage factor η decreases rapidly, thus decreasing the revolution frequency spread coming from the energy spread. Landau damping therefore diminishes and the beam is subject to instability. Below transition, most proton machines are dominated by space-charge impedance. If the resistive part of the total impedance is small, the proton bunches should be stable against microwave instability. However, as soon as transition is crossed, the space-charge force switches sign which together with the vanishingly small value of the slippage factor will drive the beam to instability. This is called *negative-mass instability*, the name coming from the fact that particle behavior above transition are the same as if they are having negative mass. All low-energy proton machines will suffer from negative-mass instability while crossing transition. However, this instability grows for a limited time only until the slippage factor η becomes large enough to damp the instability. If the ring is well-designed so that the time interval of growth and the growth rate are both small, negative-mass instability just results in a small increase in bunch area. If the ring is not well-designed, the increase in bunch area will be so large that the bunch may exceed the bucket height and even the momentum aperture of the vacuum chamber resulting in beam loss. In a machine like the Fermilab Main Ring where bunch coalescence is required to feed the Tevatron which is a colliding ring, the growth in bunch area is especially important. This is because too large a bunch area after transition will lead to undesirable large bunch area after coalescence, which will in turn lower the luminosity of the Tevatron.

As was discussed in Sec. 5.3, while the Landau damping rate decreases as η, the microwave instability growth rate decreases as $\sqrt{|\eta|}$ as well. The growth rate is therefore

time dependent, thus complicating the calculation of the total amount of growth in bunch area.

16.1 GROWTH AT CUTOFF

In the absence of space charge or other coupling impedances, the motion of a particle in the longitudinal phase space can be derived analytically [3] at any time near transition in terms of Bessel function $J_{\frac{2}{3}}$ and Neumann function $N_{\frac{2}{3}}$. With the introduction of space charge, the growth rate of a small excitation amplitude can be evaluated by integrating the Vlasov equation when the bunch has either an elliptical or bi-Gaussian distribution in the longitudinal phase space. The total growth can then be tallied up by small time steps across transition. Lee and Wang [1] made such a calculation for the Relativistic Heavy Ion Collider to be built at Brookhaven. The emittance growth was taken as two times the growth of the excitation amplitude at the cutoff frequency of the beam pipe, and the result was considered satisfactory. The choice of the cutoff frequency comes from the assumption that electromagnetic waves emitted by the bunch at higher frequencies will not bounce back from the beam pipe to interact with the bunch. Wei [2] later studied the emittance growth of the Alternating-Gradient Synchrotron at Brookhaven using similar approach. His simulation showed that the emittance blowup had been very much overestimated. Wei pointed out that the bunch emittance had been kept constant by Lee and Wang in the computation of the growth for each time step. The bunch emittance was in fact growing and would provide more Landau damping to counteract the instability. With the emittance update at each time step, he found the numerical calculations agree with the simulations.

16.1.1 SIMPLE MODEL

With some suitable assumptions, the model of Lee-Wang-Wei can be made analytic, resulting in some simple formulas for easy estimation [3]. First, let us begin with the dispersion relation derived in Chapter 5 for the revolution harmonic n:

$$1 = -\left(\frac{\Delta\Omega_0}{n}\right)^2 \int \frac{F'(\omega)}{\Delta\Omega/n - \omega}\, d\omega \ , \tag{16.1}$$

where $\Delta\Omega = \Omega - n\omega_0$ is the coherent angular frequency shift, Ω the coherent angular frequency of the instability, and ω_0 the revolution angular frequency. In above, $\Delta\Omega_0$ is

the coherent frequency shift without Landau damping, which can be expressed as

$$\left(\frac{\Delta\Omega_0}{n}\right)^2 = \frac{ie\eta\omega_0^2 I_{\rm pk}}{2\pi\beta^2 E}\,\frac{Z_0^{\|}}{n}\ , \tag{16.2}$$

and $F(\omega)$ is the revolution-frequency distribution of the beam,

$$F(\omega) = \frac{1}{\sqrt{2\pi}\sigma_\omega}\,e^{-\omega^2/(2\sigma_\omega^2)}\ , \tag{16.3}$$

with

$$\sigma_\omega = \frac{|\eta|\omega_0}{\beta^2 E}\,\sigma_{\scriptscriptstyle E} \tag{16.4}$$

the rms angular frequency spread in the bunch, $\sigma_{\scriptscriptstyle E}$ the rms energy spread, and $I_{\rm pk} = eN_b/(\sqrt{2\pi}\sigma_\tau)$ the peak current of the bunch of N_b particles and rms length $\sigma_\tau = 1/\sigma_\omega$. Dimensionless variables are now introduced,

$$u = \frac{\omega}{\sigma_\omega}\ , \qquad z = \frac{\Delta\Omega}{n\sigma_\omega}\ , \tag{16.5}$$

and the dispersion relation takes the form

$$1 = -\left(\frac{\Delta\Omega_0}{n}\right)^2 \int \frac{G'(u)}{z-u}\,du\ , \tag{16.6}$$

with

$$G(u) = \frac{1}{\sqrt{2\pi}}\,e^{-u^2/2}\ . \tag{16.7}$$

Again, we assume the slippage factor η to be linear in time near transition as given by

$$\frac{\eta}{E} = \frac{2\dot{\gamma}_t}{\gamma_t^4 E_0}\,t = \frac{eV_{\rm rf}\omega_0\sin\phi_s}{\pi\gamma_t^4 E_0}\,t\ , \tag{16.8}$$

where t is the time measured from the moment transition is crossed, E_0 the rest energy of the beam particles and $V_{\rm rf}$ the rf voltage. We get, from Eqs. (16.2), (16.6), and (16.8),

$$1 = -i\frac{a}{t}\int \frac{G'(u)}{z-u}du\ , \tag{16.9}$$

where

$$a = \frac{eN_b(Z_0^{\|}/n)\beta^2\gamma_t^4 E_0^2}{2\sqrt{2\pi}\omega_0\sigma_\tau\sigma_{\scriptscriptstyle E}^2 V_{\rm rf}\sin\phi_s}\ , \tag{16.10}$$

is a slowly varying function of t. Written in this form, all accelerator and bunch parameters have been embedded in the variable a and integral in Eq. (16.9) becomes machine and beam independent.

Next, we want to compute the time t_0 when η increases to such a value that stability is regained. There are two simple situations. The first one is when the longitudinal impedance is purely space charge or capacitive. Therefore, the parameter a is positive imaginary number or $-ia$ is real and positive. This corresponds to Point A on the threshold curve shown in Fig. 16.1. Solution of the dispersion relation, Eq. (16.9), for the

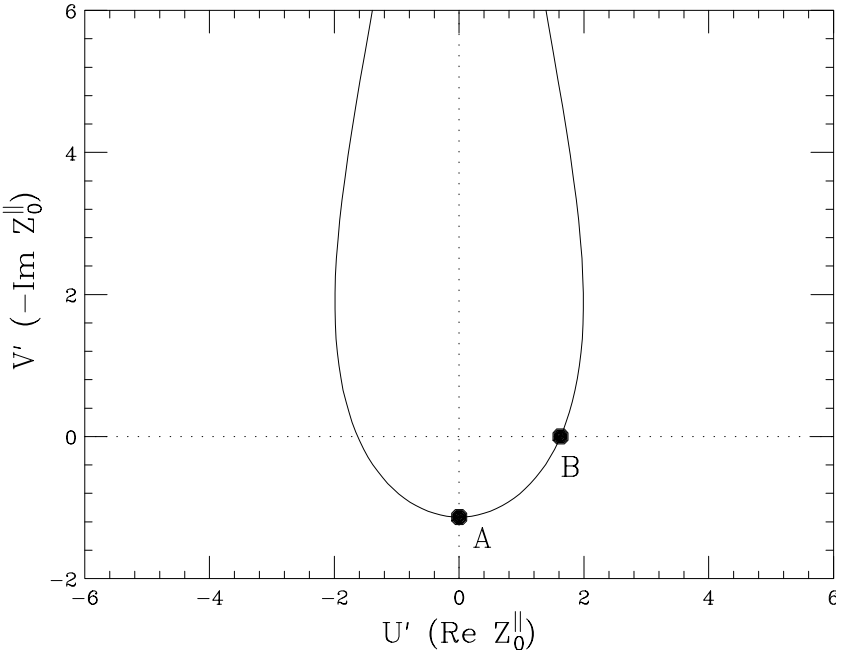

Figure 16.1: The threshold dispersion curve for Gaussian distribution. Point A corresponds to the situation where the longitudinal impedance is purely capacitive such as space charge. Point (b) corresponds to the situation where the longitudinal impedance is purely real such as the peak of a broad resonance.

threshold is simply $z = +i\epsilon$ where ϵ is a positive infinitesimal real number. The integral can be performed easily and we obtain

$$t_0 = -ia(t_0) \ . \tag{16.11}$$

We now make the approximation that $a(t) \approx a(t_0)$. The quantities of largest variation with time in $a(t)$ are σ_τ and σ_E. It turns out that t_0 in most cases is of the order of the

non-adiabatic time T_c or larger, so that the bunch area, which is conserved, is close to $S = 6\pi\sigma_\tau\sigma_E$. Thus $a(t) \propto \sigma_\tau$. We notice from Eqs. (15.19) and (15.54) that the variation of σ_τ from $t = 0$ to $t = T_c$ is at most $\sim 10\%$. Therefore, the approximation should be valid. With this approximation, we can compute from Eq (16.9) the growth rate at other time $t = t't_0$, where $0 \le t' \le 1$. The equation to solve is

$$t' = \int \frac{G'(u)}{z-u}\, du \ . \tag{16.12}$$

The solution is simple because the imaginary part of the right side has to vanish, leading to $z = iy$, where y is real. We obtain

$$t' = 1 - \sqrt{\frac{\pi}{2}}\, y\, e^{y^2/2}\, \mathrm{erfc}\left(-\frac{y}{\sqrt{2}}\right) \ , \tag{16.13}$$

where $\mathrm{erfc}(x) = 1 - \mathrm{erf}(x)$ is the complimentary error function. The integrated growth per harmonic is given by

$$\frac{S_+}{n} = \int_0^{t_0} \mathcal{I}m\, \frac{\Delta\Omega}{n}\, dt = t_0 \int_0^1 \sigma_\omega\, \mathcal{I}m\, z\, dt' = \frac{\sigma_E e V_{\rm rf} \sin\phi_s \omega_0^2 t_0^2}{\pi \beta_t^2 \gamma_t^4 E_0^2} \int_0^1 t'\, \mathcal{I}m\, z\, dt' \ . \tag{16.14}$$

In Fig. 16.2(a), we plot $t'\,\mathcal{I}m\, z$ as a function of t' with the aid of Eq. (16.13). The last integral in Eq. (16.14) is 0.10346. With the aid of Eqs. (16.10) and (16.11), the integrated growth per harmonic becomes

$$\frac{S_+}{n} = F_1^{\rm spch} \sigma_\tau \frac{\left(e^2 N_b |Z_0^\parallel/n| \beta_t \gamma_t^2 E_0\right)^2}{S^3 e V_{\rm rf} \sin\phi_s} \ , \tag{16.15}$$

where the constant is machine independent and is given by

$$F_1^{\rm spch} = 27\pi \int_0^1 t'\, \mathcal{I}m\, z\, dt' = 8.776 \ . \tag{16.16}$$

In above, we have used the fact that the 95% bunch area is $S \approx 6\pi\sigma_\tau\sigma_E$, since $t_0 \gtrsim T_c$. The rms bunch length σ_τ will be evaluated using Eq. (15.52).

Another possibility to have a simple formula is to assume $Z_0^\parallel/n$ to be purely real, for example at the peak of a broad resonance. Now the variable a in Eq. (16.9) is real and positive. Therefore, we require the real part of the dispersion integral to vanish. To derive the time t_0 where the beam regains stability, we seek the solution $z = x + i\epsilon$, where ϵ is a positive infinitesimal number. We find that x satisfies

$$1 - \frac{x}{\sqrt{2}}\, e^{-x^2/2} \int_0^{x/\sqrt{2}} e^{t^2} dt = 0 \ . \tag{16.17}$$

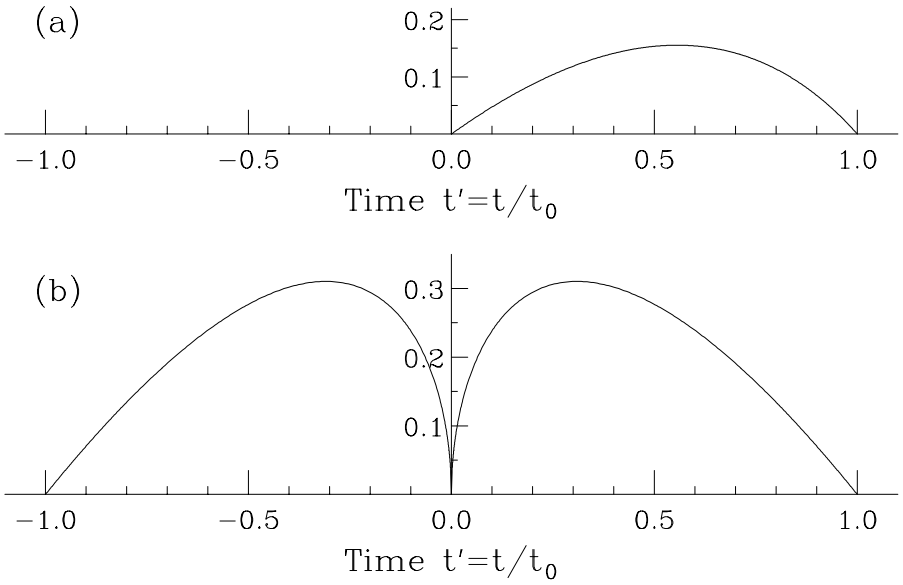

Figure 16.2: Plot of $t' \mathcal{I}m\, z$, which is proportional to the growth rate as a function of normalized time $t' = t/t_0$, where t is measured from the moment when transition is crossed ($t < 0$ below transition and $t > 0$ above transition), and t_0 is the time when the slip factor η becomes large enough so that stability is achieved. Plot (a) is the situation when the longitudinal impedance is purely capacitance like space charge. Plot (b) is the situation when the longitudinal impedance is purely real like the peak of a broad resonance. Note that there is no growth below transition when the impedance is purely capacitive.

This gives $x/\sqrt{2} = 0.69729$ or

$$t_0 = 0.697285\, a(t_0) \ . \tag{16.18}$$

Again, we approximate the problem by evaluating $a(t)$ at t_0. Substituting back into the dispersion relation, the Eq. (16.9) becomes

$$0.697285\, t' = -i \int \frac{G'(u)}{z-u}\, du = -i \left[1 + i \sqrt{\frac{\pi}{2}}\, z\, w\left(\frac{z}{\sqrt{2}} \right) \right] \ , \tag{16.19}$$

where $t' = t/t_0$ and $w(z)$ is the complex error function. Next we need to relate the growth rate, which is proportional to $\mathcal{I}m\, z$, to the time t' before stability is regained. For each value of $y = \mathcal{I}m\, z$, we require

$$1 - \mathcal{I}m \left[\sqrt{\frac{\pi}{2}}\, z\, w\left(\frac{z}{\sqrt{2}} \right) \right] = 0 \ , \tag{16.20}$$

by solving for x, where $z = x + iy$. This has to be solved numerically. The relation of $t'\,\mathcal{I}m\,z$ as a function of t' is plotted in Fig. 16.2(b). The area under the growth-rate curve is 0.211765 for $0 \le t' \le 1$. Unlike the situation of a purely capacitive impedance, there is microwave growth both after and before transition. In this particular model of a purely real impedance, the growth is symmetric about the time when transition is crossed. The integrated growth above transition per harmonic S_+/n is exactly the same expression in Eq. (16.15) when the constant $F_1^{\rm spch}$ replaced by another universal constant $F_1^{\rm real}$, where

$$F_1^{\rm real} = 27\pi(0.697285)^2 \int_0^1 t'\,\mathcal{I}m\,z\,dt' = 27\pi(0.697285)^2(0.211765) = 8.734\ , \qquad (16.21)$$

which happens to be very close to $F_1^{\rm spch}$. The integrated growth per harmonic S_-/n below transition is exactly equal to S_+/n.

When the condition that $Z_0^{\parallel}/n$ is purely reactive or real is relaxed, the solution of the dispersion relation will not be so simple. The result can also be expressed in the form of Eq. (16.15). The numerical constant F_1 will deviate from $F_1^{\rm spch}$ and $F_1^{\rm real}$. Also there will be a different F_1 for a different phase in $Z_0^{\parallel}/n$.

Here, we will apply these formulas to the Fermilab Booster, Main Ring, and Main Injector, as listed in Table 16.1. Since the total growth is exponential, it is very sensitive to the bunch area, impedance, number per bunch, and the growth harmonic. Even a factor of two decrease in the bunch area or a factor of two enhancement in one of the other quantities can increase the the total growth tremendously. Notice that some total growths are more than 10000 fold. But this is only the growth of a spectral component and it is not easy to relate it to the growth of the bunch area. For this reason, the theory of growth at cutoff is not so enlightening. We will analyze all the shortcomings of the model and study the model of Hardt [6], which may provide a more reasonable criterion of instability.

16.1.2 SHORTCOMINGS

In order to discuss the shortcomings of the Lee-Wang-Wei method, let us first review some theory of the negative-mass instability. If we ignore Landau damping, the growth rate at peak current $I_{\rm pk}$ at the revolution harmonic n is given by

$$G(n,t) = n\omega_0 \left(\frac{\eta e I_{\rm pk} |Z_0^{\parallel}/n|_{\rm spch}}{2\pi\beta^2\gamma E_0} \right)^{1/2} , \qquad (16.22)$$

Table 16.1: Growth-at-cutoff theory applied to the Fermilab Booster, Main Ring, and main Injector when the impedance is purely space charge or purely resistive.

	Booster	Main Ring	Main Injector	
95% Bunch Area S	0.025	0.15	0.15	eV-s
Number per bunch N_b	3×10^{10}	3×10^{10}	6×10^{10}	
Beam pipe radius	5.00	3.50	2.66	cm
Non-adiabatic time T_c	0.216	3.00	2.14	
Cutoff harmonic n	1510	28600	19900	
Cutoff frequency	0.938	1.36	1.79	GHz
Purely Space Charge				
$\lvert Z_0^{\parallel}/n\rvert_{\rm spch}$	30.0	2.63	1.72	Ohms
t_0	2.23	2.30	2.71	ms
σ_τ at t_0	0.463	0.342	0.251	ns
Growth rate per harmonic S_+/n	0.00619	7.40×10^{-6}	2.10×10^{-5}	
Growth index S_+	9.35	0.203	0.416	
Total growth $\exp(S_+)$	11400	1.23	1.52	
Resistive Impedance				
$Z_0^{\parallel}/n$	15.0	10.0	1.6	Ohms
t_0	0.549	8.58	1.52	ms
σ_τ at t_0	0.326	0.475	0.217	ns
Growth rate per harmonic S_+/n	0.000125	1.66×10^{-5}	1.78×10^{-6}	
Growth index $S_+ + S_-$	3.30	8.31	0.619	
Total growth $\exp(S_+ + S_-)$	27.0	4060	1.86	

where E_0 is the particle rest energy, η the slippage factor, t the time measured from the moment of transition crossing, and the space-charge impedance given by

$$\left[\frac{Z_0^{\parallel}}{n}\right]_{\rm spch} = i\frac{Z_0 g}{2\beta\gamma^2}\,. \tag{16.23}$$

Here, $Z_0 \approx 377$ ohms is the free-space impedance, γ and β the relativistic parameters of the bunch particle at or near transition, and g the space-charge geometric parameter, which has been derived in Sec. 4.2 at low frequencies as

$$g_0 = 1 + 2\ln\frac{b}{a}\,, \tag{16.24}$$

where a is the beam radius and b the beam pipe radius. A more accurate derivation which is valid for high frequencies has been given by Keil and Zotter [7] in terms of Bessel functions. The result of Eq. (16.24) arrives from the expansion of the Bessel functions at zero frequency. At frequencies of the order $\gamma c/b$, $\gamma c/a$, or higher, the space-charge geometric parameter g rolls off. When b/a is not too big, numerical fittings show that $g(n)$ can be approximated by

$$g(n) = \frac{g_0}{1 + (n/n_{\frac{1}{2}})^2} \ , \tag{16.25}$$

with the half-value harmonic given roughly by

$$n_{\frac{1}{2}} = \gamma R \left(\frac{1.6}{b} + \frac{0.52}{a} \right) \ , \tag{16.26}$$

where R is the radius of the accelerator ring. It is clear from Eq. (16.22) that at frequencies below the roll-off of the space-charge impedance, the growth rate for negative-mass instability is directly proportional to the harmonic n. It will be showed later in Eq. (16.56) that, when Landau damping is taken into account, the growth rate will be modified and the integrated growth becomes

$$\int_0^{t_0} G(n,t)\, dt \propto n g^2(n) \ , \tag{16.27}$$

where t_0 is the time after crossing transition when the slip factor η becomes large enough so that stability is restored. Thus, the integrated growth exhibits a maximum at $n_{\max} = n_{\frac{1}{2}}/\sqrt{3}$. Taking as an example the Fermilab Main Ring, which has a radius of 1 km and transition gamma $\gamma_t = 18.8$, this corresponds to 77.6 GHz when $a = 5$ mm and $b = 35$ mm. On the other hand, the cutoff frequency is only about 1.36 GHz. For a typical cycle at an intensity of 3×10^{10} per bunch and emittance 0.15 eV-s, the total growth across transition due to the space-charge impedance for a spectral line is 1.74×10^5 times at the former frequency but only 1.23 at the latter frequency. Similarly, the maximum integrated negative-mass growths for the Fermilab Main Injector and the Fermilab Booster occur at 98.5 and 23.9 GHz, respectively. As a result, it is difficult to justify the correctness of the description of Lee-Wang-Wei. In addition, in Wei's simulation, the bunch was divided into bins with the bin width equal to the cutoff wavelength of the beam pipe. In other words, all large-growth-rate amplitudes at high frequencies had been neglected. Here, we want to point out that the first simulation across transition to exhibit negative-mass instability was done by Lee and Teng [4] on the Fermilab Booster, where they also divided

the bunch up into cutoff wavelengths only. Later, similar simulations on the same booster were performed by Lucas and MacLachlan [5], and they also failed to include the high-frequency amplitudes.

Measurements were made near transition for the Fermilab Main Ring [8]. The top row of Fig. 16.3 displays the observed signals around transition at frequencies 4, 5, and 6 GHz for proton bunches with initial longitudinal emittance 0.07 eV-s and 2.3×10^{10} protons. The units on the vertical axis are 5 db per division and on the horizontal axis 2 ms per division. The transition time is marked with an arrow. As seen in the figure, the signals are getting stronger and more persistent with increasing frequency as expected from the negative-mass instability. In this case, the longitudinal emittance after transition was 0.25 eV-s corresponding to a blowup of 3.6. Next a phase mismatch at injection was introduced to blowup the longitudinal emittance from 0.06 to 0.10 eV-s. The lower row of Fig. 16.3 displays the signals observed at 5.0 GHz, with two different longitudinal emittances before transition. As expected, the 5.0 GHz signal is smaller for the bigger longitudinal emittance, and dies away faster compared to the signal in the case with the smaller emittance. The emittance blowup at transition is also much smaller for the bigger initial emittance, a factor of 2 compared with 3.7.

One may raise the question that a typical proton bunch which is usually much longer than the radius of the beam pipe will have a spectrum not much higher than the cutoff frequency. In order to have a growth at harmonic $n = n_{\max}$ or $n_{\frac{1}{2}}$, the original amplitude or the seed of the growth has to be supplied by Schottky noise, which is extremely small, so that the growth effect to the bunch at such high frequencies may or may not be significant. This question will be discussed in Sec. 16.2.1 below, after we go over the Schottky-noise model of Hardt [6].

16.2 SCHOTTKY-NOISE MODEL

Hardt assumed that the seeds of the negative-mass growth are provided by the statistical fluctuations of the finite number of particles N_b within the bunch on top of a smooth linear profile distribution $F(\Delta\phi)$, where $\Delta\phi$ is the rf phase offset measured from synchronous angle. The smooth distribution $F(\Delta\phi)$ has an average of unity but is normalized to $2\widehat{\Delta\phi}$, the total bunch length. The bunch is divided into M bins in the rf phase coordinate $\Delta\phi$. There are $N_b F(\Delta\phi)/M$ particles in the bin at $\Delta\phi$, and each bin has a width $2\widehat{\Delta\phi}/M$. Due to the statistical fluctuations, the mth bin contains δN_m extra

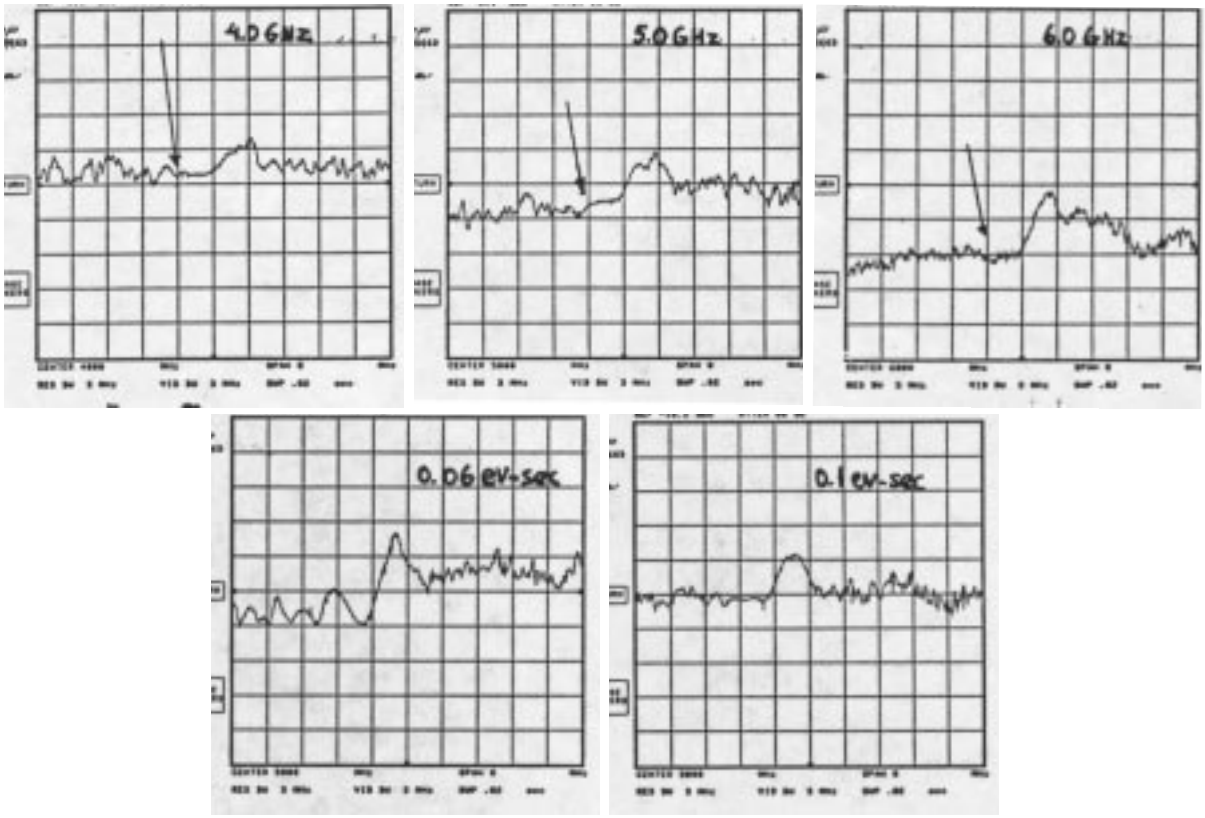

Figure 16.3: Top row: negative-mass signals at 4.0, 5.0, and 6.0 GHz for bunches with emittance of 0.07 eV-sec and 2.2×10^{10} protons. The signals are stronger and more persistent with increasing frequencies. The arrow marks the transition time. Lower row: negative-mass signals at 5.0 GHz for bunches with the same intensity but with longitudinal emittances 0.06 and 0.10 eV-s. The signals are smaller for the larger emittance.

particles. So a step function $f(\Delta\phi, t)$, which is a perturbation to $F(\Delta\phi)$, can be defined:

$$f(\Delta\phi, t) = \frac{\delta N_m}{\Delta N} \qquad \text{if} \quad \frac{m-1}{M} < \frac{\Delta\phi + \widehat{\Delta\phi}}{2\widehat{\Delta\phi}} < \frac{m}{M} \ , \tag{16.28}$$

where $\Delta N = N_b/M$ is the average number of particles in a bin. The function can be expanded in a Fourier series

$$f(\Delta\phi, t) = \sum_{k_b=-\infty}^{\infty} c_{k_b}(t) e^{i2\pi k_b \Delta\phi/(2\widehat{\Delta\phi})} \ , \tag{16.29}$$

where

$$c_{k_b}(t) = \frac{1}{2\widehat{\Delta\phi}} \int_{-\widehat{\Delta\phi}}^{\widehat{\Delta\phi}} f(\phi, t) e^{-i2\pi k_b \Delta\phi/(2\widehat{\Delta\phi})} d\Delta\phi \ , \tag{16.30}$$

and $c_0(t) = 0$ because of charge or particle conservation. Notice that the expansion has been made in bunch modes k_b, or the number of wavelengths in a wave that can reside in a bunch with periodic boundary condition at $\pm\widehat{\Delta\phi}$. It should not be confused with the revolution harmonic n, which is the number of wavelengths in a wave around the circumference of the accelerator ring. The two are, however, related to each other by

$$\frac{k_b}{n} = \frac{2\widehat{\Delta\phi}}{2\pi h} \, , \tag{16.31}$$

where h is the rf harmonic. If we work with waves that vanish at the ends of the bunch or $\pm\widehat{\Delta\phi}$, we need only to include positive integral k_b which represents the number of nodes in the waves across the bunch. However, we are working here with waves that satisfy periodic boundary conditions at $\pm\widehat{\Delta\phi}$; we need to include all integral k_b, positive and negative.

Let us compute the statistical expectation

$$E\Big[|c_{k_b}(0)|^2\Big] = \frac{1}{(2\widehat{\Delta\phi})^2} \int_{-\widehat{\Delta\phi}}^{\widehat{\Delta\phi}} d\Delta\phi \int_{-\widehat{\Delta\phi}}^{\widehat{\Delta\phi}} d\Delta\phi' \, E\left[\frac{\delta N_m \delta N_n}{(\Delta N)^2}\right] e^{i2\pi k_b(\Delta\phi - \Delta\phi')/(2\widehat{\Delta\phi})} \ . \tag{16.32}$$

Initially, without any contamination of instability, the statistical fluctuations in the bins are random, or

$$E\Big[\delta N_m \delta N_n\Big] = \delta_{mn} \, 2\widehat{\Delta\phi} \Delta N F(\Delta\phi) \ , \tag{16.33}$$

where the right side is the expected number of particles in the mth bin, in which $F(\Delta\phi)$ is to be evaluated. This means that both $\Delta\phi$ and $\Delta\phi'$ have to be in the same bin in order to be nonvanishing. If we neglect the small fluctuation of the phase inside a bin, we can perform the integration over $d\Delta\phi'$, which just gives the width of the bin. What is left behind in Eq. (16.32) becomes trivial, and we readily get

$$E\Big[|c_{k_b}(0)|^2\Big] = \frac{1}{(2\widehat{\Delta\phi})^2} \int_{-\widehat{\Delta\phi}}^{\widehat{\Delta\phi}} \frac{F(\Delta\phi)}{\Delta N} \frac{2\widehat{\Delta\phi}}{M} \, d\Delta\phi = \frac{1}{N_b} \, . \tag{16.34}$$

This result is important because it is independent of mode number k_b and the number of bins M, otherwise the model will become meaningless. This also explains why $F(\Delta\phi)$

has been defined to have an average of unity. The evolution of each mode amplitude c_{k_b} is

$$|c_{k_b}(t_0)| \approx \frac{1}{\sqrt{N_b}} \exp \int_0^{t_0/T_c} G(n,x)\, dx\,, \tag{16.35}$$

where $G(n,x)$, the growth per unit $x = t/T_c$ with T_c being the non-adiabatic time. It will be derived below in exactly the same way as what we did in the growth-at-cutoff model. The integration is up to time t_0 when the growth rate decreases to zero as the slippage factor η increases.

Hardt employed an elliptical initial particle distribution in the longitudinal phase space,*

$$\psi(\Delta\phi, \Delta E) = \frac{3}{2\pi\widehat{\Delta\phi}\widehat{\Delta E}} \sqrt{1 - \frac{\Delta\phi^2}{\widehat{\Delta\phi}^2} - \frac{\Delta E^2}{\widehat{\Delta E}^2}}\,, \tag{16.36}$$

so that the linear distribution

$$\rho(\Delta\phi) = \frac{3}{4\widehat{\Delta\phi}} \left(1 - \frac{\Delta\phi^2}{\widehat{\Delta\phi}^2}\right) \tag{16.37}$$

becomes parabolic. The offset of angular revolution frequency $\Delta\omega = \omega - \omega_0$ from that of the synchronous particle is related to the energy offset ΔE by

$$\Delta\omega = -\frac{\eta\omega_0}{\beta^2\gamma E_0}\, \Delta E\,. \tag{16.38}$$

Therefore, at a point $\Delta\phi_1$ along the bunch profile, the distribution in $\Delta\omega$ is

$$f(\Delta\omega) = \frac{2}{\pi\widehat{\Delta\omega}} \frac{\sqrt{1 - \dfrac{\Delta\phi_1^2}{\widehat{\Delta\phi}^2} - \dfrac{\Delta\omega^2}{\widehat{\Delta\omega}^2}}}{1 - \dfrac{\Delta\phi_1^2}{\widehat{\Delta\phi}^2}}\,. \tag{16.39}$$

Starting from the Vlasov equation, a dispersion relation is derived and is given by Eq. (5.16). For a perturbative wave with revolution harmonic n, the dispersion relation is

$$1 = -\left(\frac{\Delta\Omega_1}{n}\right)^2 \int \frac{df(\Delta\omega)/d\Delta\omega}{\Delta\Omega/n - \Delta\omega}\, d\Delta\omega\,, \tag{16.40}$$

*We outline here our understanding of the original paper of Hardt, which is very condensed and is difficult to read.

where $\Delta\Omega$ is the deviation of coherent angular frequency Ω of the collective motion from $n\omega_0$. We are working with the revolution harmonic now and will go to bunch modes later. The factor before the integral can be written as [Eq. (5.16)]

$$\left(\frac{\Delta\Omega_1}{n}\right)^2 = \frac{ieI_{\rm local}\eta\omega_0^2\left[Z_0^{\parallel}(\Omega)/n\right]_{\rm spch}}{2\pi\beta^2\gamma E_0} \ , \tag{16.41}$$

where we substitute for the *local* current

$$I_{\rm local} = \frac{3eN_b\omega_0}{4\widehat{\Delta\phi}}\left(1-\frac{\Delta\phi_1^2}{\widehat{\Delta\phi}^2}\right) \ , \tag{16.42}$$

and the space-charge impedance

$$\left[\frac{Z_0^{\parallel}}{n}\right]_{\rm spch} = i\frac{Z_0 g(n)}{2\beta\gamma^2} \tag{16.43}$$

with the geometric factor $g(n)$ given by Eq. (16.25). The result is

$$\left(\frac{\Delta\Omega_1}{n}\right)^2 = -\frac{3N_b r_p g\eta h\omega_0^2}{4\beta^2\gamma^3 R\widehat{\Delta\phi}}\left(1-\frac{\Delta\phi_1^2}{\widehat{\Delta\phi}^2}\right) = \left(\frac{\Delta\Omega_0}{n}\right)^2\left(1-\frac{\Delta\phi_1^2}{\widehat{\Delta\phi}^2}\right) \ , \tag{16.44}$$

where R is the radius of the accelerator ring and r_p the classical radius of the beam particle. Notice that the last factor involving $\Delta\phi_1$ will cancel the same factor in the denominator of the distribution function $f(\Delta\omega)$ in the dispersion relation.

Changing the variable of integration from $\Delta\omega$ to

$$y = \frac{\Delta\omega}{\widehat{\Delta\omega}\sqrt{1-\dfrac{\Delta\phi_1^2}{\widehat{\Delta\phi}^2}}} \ , \tag{16.45}$$

the dispersion relation simplifies to

$$1 = \frac{2}{\pi}\left(\frac{\Delta\Omega_0}{n\widehat{\Delta\omega}}\right)^2\int_{-1}^{1}\frac{ydy}{(\alpha-y)\sqrt{1-y^2}} \ , \tag{16.46}$$

where

$$\alpha = \frac{\Delta\Omega}{n\widehat{\Delta\omega}\sqrt{1-\dfrac{\Delta\phi_1^2}{\widehat{\Delta\phi}^2}}} \ . \tag{16.47}$$

The integral on the right side of Eq. (16.46) can be readily performed to give $-\pi + \pi\alpha/\sqrt{\alpha^2-1}$. We therefore obtain

$$\alpha = \pm\frac{a}{\sqrt{a^2-1}}\ , \qquad \text{with} \quad a = 1 + \left(\frac{n\widehat{\Delta\omega}}{\sqrt{2}\Delta\Omega_0}\right)^2\ . \tag{16.48}$$

Now the dispersion relation has been solved. The imaginary part of Ω gives the growth rate if positive and damping rate if negative. It is clear from Eqs. (16.47) and (16.48) that the growth rate will be largest at the center of the bunch profile where $\Delta\phi_1 = 0$. From now on we are going to concentrate on the bunch center and drop $\Delta\phi_1$.

The maximum half spread in angular revolution frequency $\widehat{\Delta\omega}$ can be written in terms of the half bunch length $\Delta\phi$ via

$$\widehat{\Delta\omega} = \frac{|\eta|\omega_0\widehat{\Delta E}}{\beta^2\gamma E_0} = \frac{|\eta|\omega_0 S_c}{\pi\beta\gamma\widehat{\Delta\phi}}\ , \tag{16.49}$$

where, for convenience, the dimensionless bunch area $S_c = \pi\widehat{\beta\gamma}\widehat{\Delta\phi}$ [Eq. (15.96)] has been used. Thus,

$$\left(\frac{n\widehat{\Delta\omega}}{\sqrt{2}\Delta\Omega_0}\right)^2 = -\frac{2\eta\gamma R S_c^2}{3\pi^2 r_p g N_b \widehat{\Delta\phi}}\ . \tag{16.50}$$

Notice that this is essentially the inverse of the bunch length multiplied by the space-charge force.

Since we are after the growth of each bunch mode component near transition, all quantities including the bunch length will be approximated by their values at transition. Recall that under the assumption of a linear time variation of η/E, we defined in Sec. 15.5 a normalized space-charge parameter η_{N0} in Eq. (15.95) and a normalized half bunch length θ in Eq. (15.94). Here, we want to introduce η_N which is the same as η_{N0} with the exception that the space-charge geometric parameter g_0 at zero frequency is replaced by the more general $g(n)$ which covers high frequencies. With the expression in Eq. (16.50), it just turns out that

$$\left(\frac{n\widehat{\Delta\omega}}{\sqrt{2}\Delta\Omega_0}\right)^2 = -\frac{x}{\eta_N\theta}\ , \tag{16.51}$$

where $x = t/T_c$ and T_c is the non-adiabatic time. The maximum half spread in angular revolution frequency can also be expressed in terms of θ via Eqs. (15.94) and (16.49) as

$$\widehat{\Delta\omega} = \frac{|\eta|\gamma_t}{\theta\beta_t}\sqrt{\frac{S_c\omega_0}{2\pi h\dot{\gamma}_t}} = \frac{|x|}{\theta\gamma_t^2\beta_t}\sqrt{\frac{2S_c\omega_0\dot{\gamma}_t}{\pi h}}\ , \tag{16.52}$$

where the linear dependency of η near transition has been used.

With the help of Eqs. (16.47), (16.48), and (16.51), the growth rate (for $x > 0$) can be expressed as

$$\mathcal{I}m\,\Omega = n\widehat{\Delta\omega}\,\mathcal{I}m\,\alpha = n\widehat{\Delta\omega}\,\frac{\dfrac{\eta_N\theta}{x} - 1}{\sqrt{\dfrac{2\eta_N\theta}{x} - 1}}\ . \tag{16.53}$$

Now substitute for $\widehat{\Delta\omega}$ from Eq. (16.52) and the definition of the non-adiabatic time. We arrive at the growth per unit $x = t/T_c$,

$$G(n,x) = T_c\,\mathcal{I}m\,\Omega = \frac{n\eta_N}{h}\sqrt{\frac{S_c|\tan\phi_s|}{\pi\dot{\gamma}_t T_c}}\,\frac{1 - \dfrac{x}{\eta_N\theta}}{\sqrt{\dfrac{2\eta_N\theta}{x} - 1}}\ . \tag{16.54}$$

As a reminder, on the right side of the above equation, n is the revolution harmonic while η_N is the normalized space-charge parameter. The accumulated or integrated growth $E_{\rm acc}$ is obtained by an integration over x from $x = 0$ to $x = \eta_N\theta$ when the growth rate drops to zero ($t_0 = \eta_N\theta T_c$); or

$$E_{\rm acc}(n) = \int_0^{\eta_N\theta} G(n,x)\,dx\ . \tag{16.55}$$

The integration can be performed easily with the change of variable $u = x/(2\eta_N\theta)$, and the result is

$$E_{\rm acc}(n) = \frac{n\eta_N^2\theta}{h}\,\left(1 - \frac{\pi}{4}\right)\sqrt{\frac{S_c|\tan\phi_s|}{\pi\dot{\gamma}_t T_c}}\ . \tag{16.56}$$

We have computed the accumulated growth of a spectral line with revolution harmonic n. Since the normalized space-charge parameter η_N is linear in the geometric parameter $g(n)$ of the space-charge impedance, the dependence on frequency is therefore

$$E_{\rm acc}(n) \propto \frac{n}{\left(1 + \dfrac{n^2}{n_{\frac{1}{2}}^2}\right)^2}\ . \tag{16.57}$$

The maximum is denoted by

$$E_{\rm max} = \frac{3\sqrt{3}\,n_{\frac{1}{2}}\eta_{N0}^2\theta}{16h}\,\left(1 - \frac{\pi}{4}\right)\sqrt{\frac{S_c|\tan\phi_s|}{\pi\dot{\gamma}_t T_c}}\ , \tag{16.58}$$

where η_{N0} is the same as η_N with the exception of the replacement of $g(n)$ by g_0, and occurs when $n = n_{\max} = n_{\frac{1}{2}}/\sqrt{3}$. The accumulated growth $E_{\rm acc}$ will be exponentiated to arrive at the total growth for a harmonic.

A criterion for negative-mass instability is required. Hardt made the assertion that there is no negative-mass blowup if

$$\sum_{k_b=-\infty}^{\infty} |c_{k_b}(t_0)|^2 \lesssim 1\,, \tag{16.59}$$

where t_0 is the time when stability is regained. The meaning of this criterion will be explored later. From Eq. (16.35), such a criterion is equivalent to

$$\sum_{k_b=-\infty}^{\infty} \exp\Big[2E_{\rm acc}(k_b)\Big] \lesssim N_b\ , \tag{16.60}$$

where N_b is the number of particles in the bunch and the summation is over all possible bunch modes. Because $\exp\left[E_{\rm acc}\right]$ assumes a maximum at $n = n_{\max}$ and falls off rapidly later, the method of steepest decent will be employed. First, we find that[†]

$$E_{\rm acc}(n) \approx E_{\max}\left[1 - \left(\frac{3\Delta n}{2n_{\frac{1}{2}}}\right)^2\right]\ , \tag{16.61}$$

with $\Delta n = n - n_{\max}$. Next, the summation over all the bunch modes is converted into an integral

$$\sum_{k_b=-\infty}^{\infty} \exp\Big[2E_{\rm acc}(k_b)\Big] = \exp\left[2E_{\max}\right] \int_{-\infty}^{\infty} \exp\left[-2\left(\frac{3\sqrt{E_{\max}}\Delta k_b}{2k_{b\frac{1}{2}}}\right)^2\right] d\Delta k_b\ , \tag{16.62}$$

where the bunch mode number k_b has been used instead of the revolution harmonic n. The relation between the two are given by Eq. (16.31). In particular the half-value bunch mode is

$$k_{b\frac{1}{2}} = \frac{\widehat{\Delta\phi}}{\pi h}\, n_{\frac{1}{2}}\ . \tag{16.63}$$

The criterion of no blowup can be written as

$$E_{\max} \lesssim E_{\rm crit}\ , \tag{16.64}$$

[†]In Eq. (16.61), we obtain $[3\Delta n/(2n_{\frac{1}{2}})]^2$ for the second order term, while it is $[3\Delta n/(4n_{\frac{1}{2}})]^2$ in Ref. [6], which we think is incorrect. Therefore, we are getting slightly different results for Eqs. (16.62), (16.65), and (16.66).

where the critical total growth $E_{\rm crit}$ is obtained through Eq. (16.60) by equating the right side of Eq. (16.62) to N_b; or

$$\frac{k_{b\frac{1}{2}}}{3}\sqrt{\frac{2\pi}{E_{\rm crit}}}\exp\left[2E_{\rm crit}\right] = N_b \ , \tag{16.65}$$

after performing the Gaussian integration. This is a transcendental equation which can be solved by iteration, giving

$$E_{\rm crit} \approx \frac{1}{2}\left[\ln N_b - \ln\left(\frac{2k_{b\frac{1}{2}}}{3}\sqrt{\frac{\pi}{\ln N_b}}\right)\right] . \tag{16.66}$$

Finally, we will write out the criterion of no negative-mass blowup, Eq.(16.64), in terms of the more familiar parameters of the accelerator ring and the particle bunch. First, let us list the relevant expressions. They are the normalized space-charge parameter at zero frequency

$$\eta_{N0} = \frac{3\pi^2 N_b r_p g_0 h}{2RS_c^{3/2}}\sqrt{\frac{h\omega_0}{2\pi\beta_t\dot{\gamma}_t}} = \frac{3\pi^2 N_b r_p g_0}{2RS^{3/2}\omega_0}\sqrt{\frac{E_0^3\beta_t^2}{2\pi\dot{\gamma}_t}} \ , \tag{16.67}$$

and the normalized half bunch length at transition

$$\theta = \sqrt{\frac{\pi\beta_t\gamma_t^4}{2h\omega_0\dot{\gamma}_t T_c^2 S_c}}\,\widehat{\Delta\phi} = \frac{2\sqrt{\pi}}{3^{1/3}\Gamma\left(\frac{1}{3}\right)} = 0.91749 \ . \tag{16.68}$$

where the conversion, $S_c/S = h\omega_0/(\beta_t E_0)$ has been used. Substituting into the expression for $E_{\rm max}$ in Eq. (16.58), the threshold for no negative-mass blowup [Eq. (16.64)] can be formulated by introducing a critical parameter c less than unity in the following expression:

$$\xi\, n_{\rm max}\left(\frac{r_p}{R}\right)^2\left(\frac{E_0^{5/2}\beta_t^{7/6}}{h^{1/3}\omega_0^{4/3}\gamma_t^{2/3}}\right)\left(\frac{N_b^2 g_0^2|\tan\phi_s|^{1/3}}{S^{5/2}\dot{\gamma}_t^{7/6}}\right) = cE_{\rm crit} \ . \tag{16.69}$$

When the critical parameter $c < 1$, there is no blowup. In above, the coefficient ξ is

$$\xi = \frac{3^{25/6}\pi^2\Gamma\left(\frac{2}{3}\right)}{2^{41/6}}\left(1-\frac{\pi}{4}\right) = 2.44656 \ , \tag{16.70}$$

where $\Gamma\left(\frac{2}{3}\right) = 1.354118$ is the Gamma function, r_p the classical proton radius, E_0 the proton rest energy, R the ring radius, g_0 the geometric space-charge parameter at zero frequency, S bunch area in eV-s, ϕ_s the synchronized rf phase, γ_t the transition gamma,

$\dot{\gamma}_t$ the rate at which transition is crossed, $n_{\max}$ the revolution harmonic at which the accumulated growth is a maximum, which is related to the half-value revolution harmonic by $n_{\max} = n_{\frac{1}{2}}/\sqrt{3}$, and $k_{b\frac{1}{2}}$ the half-value bunch mode which is given by $k_{b\frac{1}{2}} = n_{\frac{1}{2}}\widehat{\Delta\phi}/(\pi h)$. We have written Eq. (16.69) in such a way that the last factor on the left side pertains to the properties of the beam while the two factors in front pertain to the properties of the accelerator ring.

Some comments are in order:
(1) The critical condition $\sum_{k_b} |c_{k_b}(t_0)|^2 = 1$ implies, through Parseval theorem, that

$$\frac{1}{2\widehat{\Delta\phi}} \int |f(\Delta\phi, t_0)|^2 d\Delta\phi = 1\,. \tag{16.71}$$

From the definition of the function $f(\Delta\phi)$, the above integral can be re-written as summation over the M bins,

$$\sum_m \left(\frac{\delta N}{\Delta N}\right)_m^2 \frac{(\Delta\phi)_b}{2\widehat{\Delta\phi}} = \sum_m \left(\frac{\delta N}{\Delta N}\right)_m^2 \frac{1}{M}\,, \tag{16.72}$$

where ΔN is the average number of particles inside each bin and $(\Delta\phi)_b$ is the width of the bin. Then Eq. (16.71) becomes

$$\frac{\sum_m (\delta N)_m^2}{M} = (\Delta N)^2\ . \tag{16.73}$$

Thus, the assertion of a negative-mass blowup is equivalent to the situation when the rms fluctuation in each bin is comparable to the average number of particles in each bin, which is really a large particle fluctuation or a big blowup in the bunch. This blowup implies violent changes in the bunch, such as a total bunch breakup. However, the assertion of Eq. (16.59) is a bit hand-waving, because even when the rms fluctuation is much less than ΔN, there can be a big blowup of the bunch emittance already. Hardt's paper provides no recipe to compute the increase in bunch emittance in this regime.

(2) The derivation so far has been a perturbative approach. Here, we want to examine its validity. The perturbation expansion is, in fact,

$$F(\Delta\phi) + f(\Delta\phi, t) = F(\Delta\phi) + \sum_{k_b=-\infty}^{\infty} c_{k_b}(t) e^{i2\pi k_b \Delta\phi/(2\widehat{\Delta\phi})}\,, \tag{16.74}$$

where $F(\Delta\phi)$ is the smooth linear profile distribution and $f(\Delta\phi, t)$ represents the fluctuation from the smooth distribution. Notice that the unperturbed distribution $F(\Delta\phi)$

has an average of unity. Since Hardt only studied the situation of no blowup or when the fluctuation function $f(\phi, t)$, as demonstrated in Eq. (16.71), has a rms of less than unity, the perturbation is therefore justified although the amount of growths of the c_{k_b}'s from $t = 0$ to $t = t_0$ are tremendous.

We are going to apply this Schottky-noise model to the Fermilab Main Ring, where many properties have been listed in Tables 15.1 and 16.1. Here, we want to study the negative-mass instability when the ramping rate across transition is $\dot{\gamma}_t = 90.0\ \mathrm{s}^{-1}$. Table 16.2 lists the computed critical parameter c for a bunch of $N_b = 2.2 \times 10^{10}$ protons and a bunch of 4.0×10^{10} protons for various bunch areas according to Eq. (16.69). The half bunch length is evaluated right at transition. This is also plotted in Fig. 16.4. We see that the parameter c increases very fast as the bunch area shrinks to a certain size. In any case, there should not be any negative-mass blowup when the bunch area is around 0.15 eV-s, as demonstrated by experiment. Similar plots for the Fermilab Main Injector and Booster are shown in Figs. 16.5 and 16.6.

Table 16.2: Critical parameter c for negative-mass instability for a proton bunch in the Fermilab Main Ring with $N_b = 2.2 \times 10^{10}$ or 4.0×10^{10} particles. The ramp rate across transition is $\dot{\gamma}_t = 90.0\ \mathrm{s}^{-1}$. A value of $c \gtrsim 1$ implies negative-mass blowup.

Bunch area	Half bunch width	$N_b = 2.2 \times 10^{10}$		$N_b = 4.0 \times 10^{10}$	
(eV-s)	(ns)	c	E_{crit}	c	E_{crit}
0.040	0.439	3.84	10.23	12.70	10.54
0.050	0.490	2.21	10.18	7.31	10.48
0.060	0.537	1.41	10.13	4.65	10.44
0.070	0.580	0.96	10.09	3.18	10.40
0.080	0.620	0.69	10.06	2.28	10.36
0.100	0.693	0.40	10.00	1.31	10.31
0.120	0.760	0.25	9.96	0.84	10.26
0.140	0.820	0.17	9.92	0.57	10.22
0.160	0.877	0.12	9.89	0.41	10.19
0.180	0.930	0.09	9.86	0.31	10.16
0.200	0.981	0.07	9.83	0.24	10.13
0.220	1.028	0.06	9.81	0.19	10.11
0.240	1.074	0.05	9.78	0.15	10.09

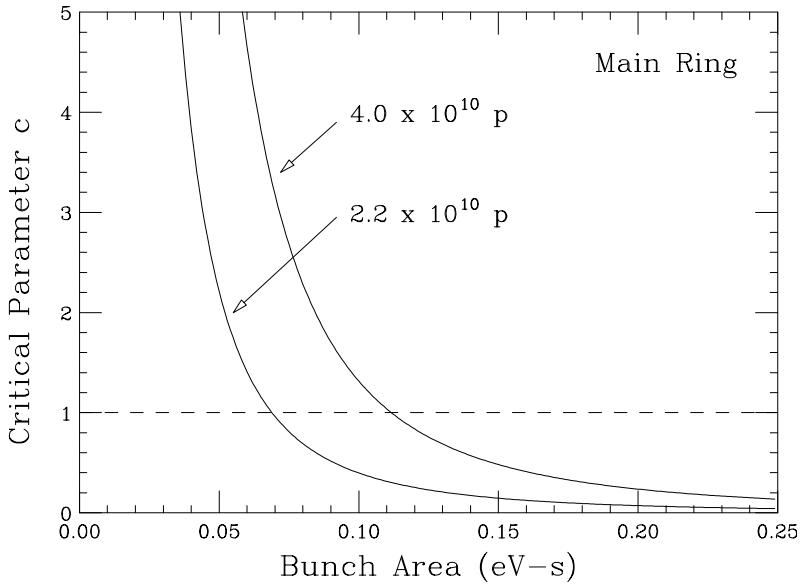

Figure 16.4: Plots showing the critical negative-mass parameter c as a function of the Fermilab Main Ring bunch area for bunches with $N_b = 2.2 \times 10^{10}$ and 4.0×10^{10} protons. The ramp rate across transition is $\dot{\gamma}_t = 90.0$ s^{-1}. Negative-mass blowup occurs when $c \gtrsim 1$.

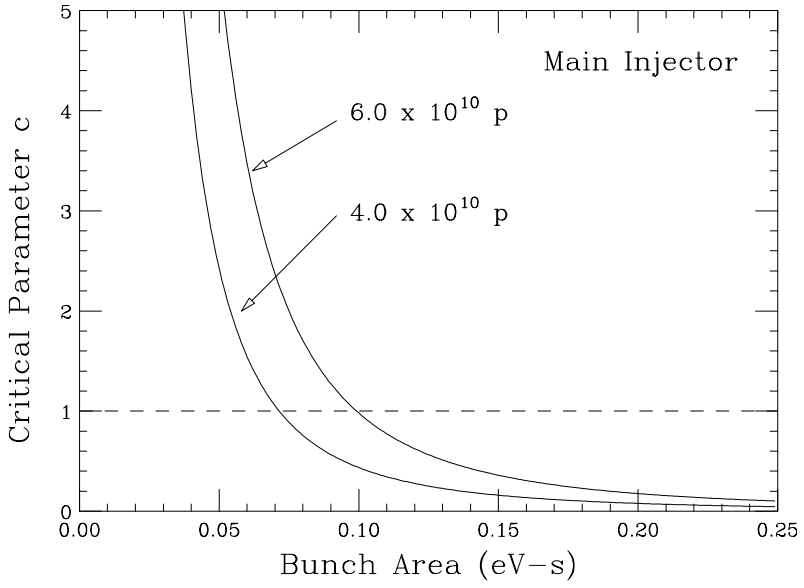

Figure 16.5: Plots showing the critical negative-mass parameter c as a function of the Fermilab Main Injector bunch area for bunches with $N_b = 4.0 \times 10^{10}$ and 6.0×10^{10} protons. The ramp rate across transition is $\dot{\gamma}_t = 160.1$ s^{-1}. Negative-mass blowup occurs when $c \gtrsim 1$.

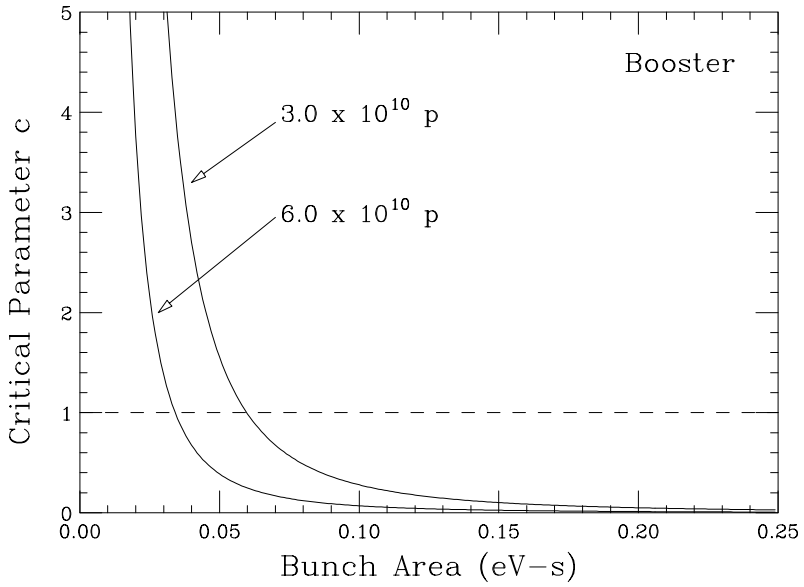

Figure 16.6: Plots showing the critical negative-mass parameter c as a function of the Fermilab Booster bunch area for bunches with $N_b = 3.0 \times 10^{10}$ and 6.0×10^{10} protons. The ramp rate across transition is $\dot{\gamma}_t = 406.7\ \mathrm{s}^{-1}$. Negative-mass blowup occurs when $c \gtrsim 1$.

16.2.1 COMPARISON OF GROWTHS AT CUTOFF AND HIGH FREQUENCIES

For a parabolic bunch, the unperturbed linear distribution is

$$F(\Delta\phi) = \frac{3}{2}\left(1 - \frac{\Delta\phi^2}{\widehat{\Delta\phi}^2}\right), \tag{16.75}$$

which is normalized to have an average of unity. It is expanded in a Fourier series at $t = 0$,

$$F(\Delta\phi) = \sum_{k_b=-\infty}^{\infty} \bar{a}_{k_b}(0) e^{i2\pi k_b \Delta\phi/(2\widehat{\Delta\phi})}, \tag{16.76}$$

where the mode amplitude is, for $k_b > 0$,

$$a_{k_b}(0) = \bar{a}_{k_b}(0) + \bar{a}_{-}k_b(0) = \frac{3}{\pi^2}\frac{(-1)^{k_b+1}}{k_b^2}. \tag{16.77}$$

The bunch mode number k_b which corresponds to the cutoff harmonic $n_{\mathrm{cutoff}} = R/b$, with R and b being, respectively, the radii of the ring and the beam pipe, can be estimated

Table 16.3: Final fluctuation power spectra at cutoff and high-frequency Schottky harmonics.

$\dot{\gamma}_t$ (s^{-1})	N_b (10^{10})	Initial Bunch Emittance (eV-s)	Final Power Spectrum of Fluctuation at $n_{\rm cutoff}$	at $n_{\rm max}$	sum
90	2.2	0.05	3.70	1.50×10^{9}	4.03×10^{10}
90	2.2	0.06	2.21	1.08×10^{2}	3.97×10^{3}
90	2.2	0.07	1.67	1.19×10^{-2}	5.74×10^{-1}
90	2.2	0.08	1.41	4.86×10^{-5}	2.93×10^{-3}
90	2.2	0.09	1.26	1.41×10^{-6}	1.06×10^{-4}
120	4.0	0.06	7.44	4.37×10^{18}	1.00×10^{20}
120	4.0	0.07	3.80	1.94×10^{9}	5.83×10^{10}
120	4.0	0.08	2.54	4.40×10^{3}	1.67×10^{5}
120	4.0	0.09	1.95	1.02×10^{0}	4.76×10^{1}
120	4.0	0.10	1.64	3.57×10^{-3}	2.00×10^{-1}

using Eq. (16.31). Then, the final value of a power spectral line can be computed:

$$|a_{k_b}(t_0)|^2 = |a_{k_b}(0)|^2 \exp\left[\int_0^{t_0/T_c} 2G(n_{\rm cutoff}, x)dx\right] . \tag{16.78}$$

The results are listed in Table 16.3 for various run cycles of the Fermilab Main Ring. The beam pipe radius and the beam radius are kept fixed at $b = 35$ mm and $a = 5$ mm, respectively. The synchronous phase is 60°. Alongside, we have also tabulated the final size of the Schottky power spectral line at the high harmonic $n_{\rm max}$ according to Eq. (16.35). The sum of all the Schottky power spectral modes has been derived in Eqs. (16.35), (16.62), and (16.65) to be

$$\sum_{k_b=-\infty}^{\infty} |c_{k_b}(t_0)|^2 \approx |c_{k_b}(t_0)|^2_{n=n_{\rm max}} \times \frac{k_{b\frac{1}{2}}}{3} \left(\frac{2\pi}{E_p}\right)^{\frac{1}{2}} , \tag{16.79}$$

where

$$E_p = \int_0^{t_0/T_c} G(n_{\rm max}, x)dx \tag{16.80}$$

is the integrated growth at the peak harmonic $n_{\rm max}$. This is also listed in the last column of the table.

We can see that the Hardt's blowup criterion of Eq. (16.59) appears to be critical,

where the growth changes tremendously. When that criterion is exceeded, the Schottky modes are always larger than the mode at cutoff, showing that the inclusion up to cutoff frequency is inadequate. On the other hand, below the blowup limit, the mode at cutoff is larger than the high-frequency Schottky modes, implying that there should be modest emittance growth below the Hardt's blowup limit. However, this does not tell us how large the emittance growth is. It will be best if we can sum up the final power spectrum of the bunch distribution:

$$\sum_{k_b} |a_{k_b}(t_0)|^2 = \sum_{k_b} \frac{9}{\pi^4 k_b^4} \exp\Big[\text{integrated growth}\Big] . \tag{16.81}$$

Unfortunately, this sum is divergent because the integrated growth is directly proportional to k_b. Even when we take into account of the space-charge roll-off, the sum still becomes unreasonably large. The reason behind this is the breakdown of the linear perturbation when the perturbed spectral mode becomes larger than the unperturbed one. As a result, it remains unclear whether the high-harmonic Schottky noise is dominating in the growth of the bunch emittance. A simulation seems to be the best solution.

16.2.2 DIFFICULTIES IN SIMULATION

A simulation of the negative-mass instability is not trivial. There are two main difficulties:

(1) Inclusion of high-frequency components

The growth of the Schottky noise peaks at $n_{\max}$, which corresponds to roughly 78 GHz for the Fermilab Main Ring, while the half-value space-charge roll-off harmonic $n_{\frac{1}{2}}$ corresponds to 134 GHz. Therefore, in simulations we need a bin size of about $1/(2 \times 134)$ or 0.00373 ns. The tracking code ESME [9] developed at Fermilab divides the whole rf wavelength or 18.8 ns up into 2^n bins where n is an integer, and the number of bins will have to be at least 4096 which is too large. As a rule of thumb, the bins should have a width less than a/γ, where a is the beam radius. Simulations of the Main Ring across transition had been performed using ESME. As we increase the bin number from 128 to 256 and 512, we do see self-bunching in the phase plot corresponding to the highest frequency of 3.40, 6.81, and 13.6 GHz, respectively, in each of the situations, as illustrated in Fig. 16.7. This suggests that the negative-mass growths at the high Schottky frequencies do play a role across transition [10]. In an actual simulation, the space-charge force is usually implemented by a differentiation of the bunch profile. To maintain the same numerical

accuracy, we need to follow the "three-in-one rule," [11] which states that whenever the bin width is reduced by a factor of 2, the number of macro-particles needs to be increased by a factor of 2^3. As a result, the tracking time will increase by a factor of 2^4.

However, a typical Main Ring bunch has a full length of only 1 ns at transition. If we divide just two or three times the bunch region into bins, there will be only 256 or 512 bins, which will reduce the tracking time drastically. Sørenssen [12] had successfully performed simulation with a bin width of a/γ. But he did not overcome the second difficulty that we are going to discuss next.

(2) The right amount of Schottky noise

In a simulation of microwave instability, there is usually ample time for the instability to develop to saturation. Therefore, we do not care so much about the size of the initial excitation or seed of the growth. Across transition, however, the bunch is negative-mass unstable only for a short time until the frequency-flip parameter η becomes large enough to provide enough Landau damping, and this time is typically of the order of the non-adiabatic time, which is about 3 ms for the Fermilab Main Ring. Therefore, the initial excitation amplitude needs to be tailored exactly. To have the exact Schottky noise level, we need to use in the simulation micro-particles instead of macro-particles. The Fermilab Main Ring bunch has typically $N_b = 2.2 \times 10^{10}$ particles, which is certainly unrealistically too many in a simulation.

A suggestion is to populate the bunch by N_M macro-particles according to a Hammersley sequence [13] instead of randomly. This is a population according to some pattern so that the statistical fluctuation will become much less. In fact, the number of particles in each bin in excess of the smooth distribution will become $\mathcal{O}(1)$ initially, or the fluctuation function defined in Eq. (16.28) starts from $f(\Delta\phi, 0) \approx 1/\Delta N_M = M/N_M$, where M is the number of bins and $\Delta N_M = N_M/M$ is the average number of macro-particles per bin. The expectation of the initial bunch mode amplitude turns out to be

$$E\Big[|c_{k_b}(0)|^2\Big] = \frac{M}{N_M^2}\,. \tag{16.82}$$

Comparing with Eq. (16.34) for a randomly distributed bunch, the required number of macro-particles becomes

$$N_M = (MN_b)^{\frac{1}{2}}\,, \tag{16.83}$$

which is more reasonable (~ 2.4 to 3.6×10^6), but may be still too large to be managed in a simulation.

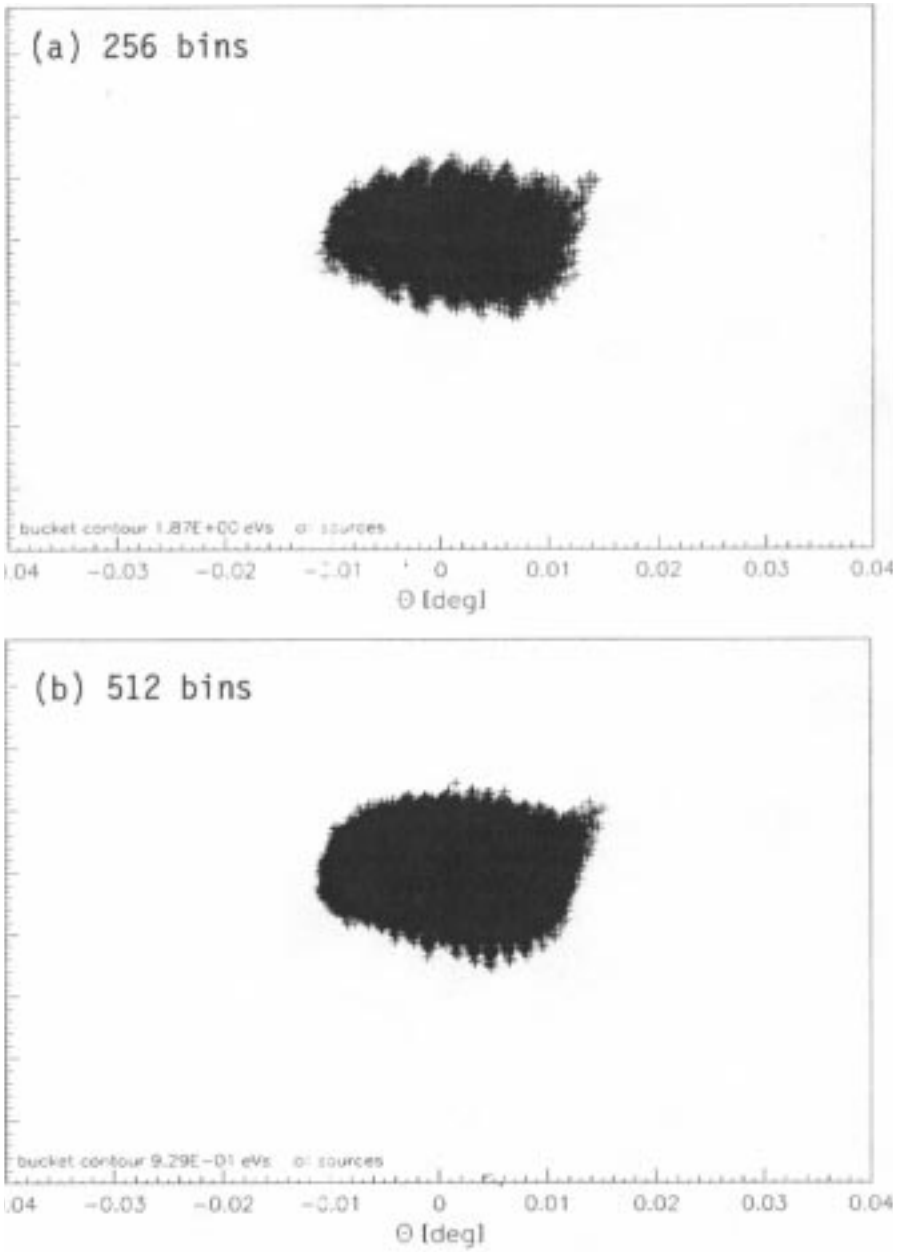

Figure 16.7: ESME simulations of a Fermilab Main Ring bunch containing 4×10^{10} particles with initial emittance of 0.1 eV-sec just after transition with (a) 256 bins and (b) 512 bins in an rf wavelength; 20,000 and 160,000 macro-particles have been used in the two cases. Excitations of 6.81 and 13.6 GHz corresponding to the respective bin widths are clearly seen in the two plots.

There are, however, two other difficulties with the Hammersley-sequence method. With $\Delta\phi$ inside the mth bin, the step function $f(\Delta\phi, t)$ has an initial expectation of

$$E\Big[f^2(\Delta\phi_m, 0)\Big] = \frac{M^2}{N_b} F(\Delta\phi)\,, \tag{16.84}$$

which is proportional to the initial unperturbed bunch distribution $F(\Delta\phi)$ and $\Delta N = N_b/M$ is the average number of micro-particles in each bin. Now it changes to, for the Hammersley population, $E[f^2(\Delta\phi, 0)] = (M/N_M)^2$ which is independent of $F(\Delta\phi)$. Thus, the relative fluctuations in the bins cannot be made to resemble those in the randomly populated bunch, and the initial fluctuation spectrum would have been altered.

In order to have the bunch to fit the space-charge modified rf bucket before transition, we usually switch on the space-charge force adiabatically over many synchrotron periods so that the initial populated bunch emittance will be preserved. However, the favored Hammersley statistics can often be lost after several synchrotron oscillations. A test was performed with 2×10^5 particles in a truncated bi-Gaussian distribution. The bunch was projected onto one coordinate, where it was divided into 20 equal bins. To simulate synchrotron oscillation, the bunch was then rotated in phase space with an angular velocity which decreases linearly by 1% from the center to the edge of the bunch. The fluctuation or number of particles in excess of the smooth projected Gaussian distribution in each bin was recorded for every rotation, and the rms was computed. The results are plotted in Fig. 16.8 as a function of rotation number. We see that although the rms fluctuation starts from 7 initially, it increases rapidly to ~ 12 after 5 rotations, ~ 20 after 20 rotations, and will approach its statistical value of 100 eventually. This might have been an overestimation, because the actual decrease in synchrotron frequency is not linear and the decrease near the core of the bunch where most particles reside is very much slower. Nevertheless, this test gives us an illustration of restoration to randomness. To cope with the fast restoration to randomness, one possibility is to compute exactly the initial distribution of the bunch in the space-charge modified rf bucket right at transition and populate the bunch according to a Hammersley sequence. In this way, the tracking of the bunch particles across the negative-mass unstable period, which is usually of the order of one synchrotron period, may reveal the reliable growth from the correct Schottky noise level.

16.3 SELF-BUNCHING MODEL

Microwave instability can be viewed as self-bunching. The beam current $I_{\rm pk}$, seeing the impedance Z_I, gives rise to an rf voltage $I_{\rm pk}Z_I$, and creates a self-bunching rf bucket

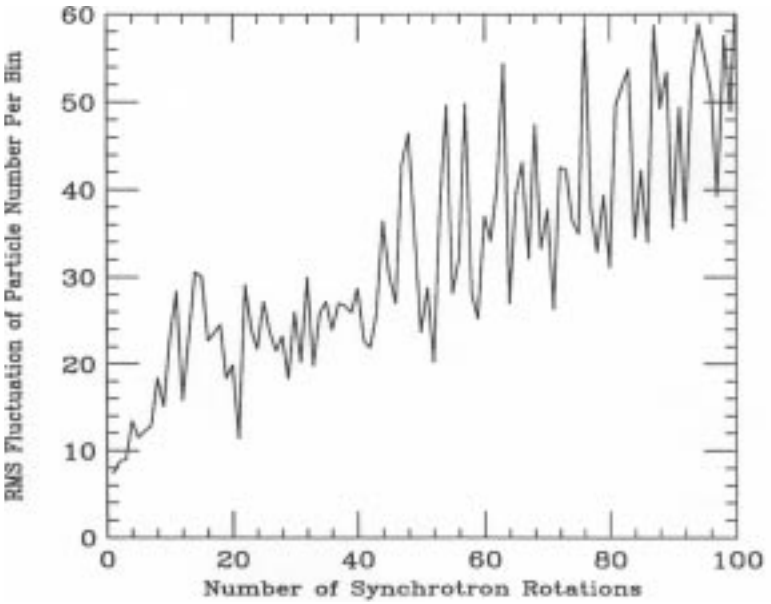

Figure 16.8: Plot of rms fluctuation of excess particles per bunch versus number of synchrotron rotations, showing the rapid loss of Hammersley statistics and restoration to randomness.

with an energy half height

$$\frac{\Delta E}{E} = \left(\frac{2\beta^2 e I_{\rm pk} Z_I}{\pi \eta n_{\rm max} \gamma E_0} \right)^{\frac{1}{2}} , \tag{16.85}$$

where $n_{\rm max}$ denotes the revolution harmonic of the impedance. If this bucket height is less than the energy spread of the bunch, there will not be any extra energy spread and the bunch will be stable. If the bucket height is larger than the energy spread of the bunch, the bunch particles will travel outside the original energy boundary of the bunch, giving rise to an emittance growth as a result of filamentation. In fact, this is just another way of expressing the Keil-Schnell criterion [14].

Here, we want to make the conjecture that this self-bunching bucket height determines the final energy spread of the bunch. Inside this bucket, the angular synchrotron frequency is given by

$$\omega_s = \left(\frac{n_{\rm max} \eta I_{\rm pk} Z_I}{2\pi \beta^2 \gamma E_0} \right)^{\frac{1}{2}} \omega_0 \, . \tag{16.86}$$

Since the frequency-flip parameter η is changing rapidly at transition, we substitute

$$\frac{\eta}{\gamma} = \frac{2\dot{\gamma}_t}{\gamma_t^4} \, t \, . \tag{16.87}$$

Integrating Eq. (16.86), we obtain the time to reach a quarter of a synchrotron oscillation from the moment of transition crossing as

$$T \approx \left(\frac{3\pi}{4}\right)^{\frac{2}{3}} \left(\frac{\pi E_0 \beta_t^2 \gamma_t^4}{n_{\max} I_{\rm pk} Z_I \dot{\gamma}_t \omega_0^2}\right)^{\frac{1}{3}} . \tag{16.88}$$

This will be the time required for some particles to reach the top of the bucket. Of course, the height of the self-bunching bucket is also changing, and the value of $\eta\gamma$ at this moment should be substituted in Eq. (16.85). At this moment, the unperturbed energy spread of an elliptical bunch with emittance S and without space-charge distortion is, from Eq. (15.79),

$$\frac{\Delta E}{E} = \frac{\Gamma\left(\frac{1}{3}\right)}{2^{1/2}3^{1/6}\pi} \left(\frac{S\beta_t^2\gamma_t^2}{E_0 T_c^2 \dot{\gamma}_t}\right)^{\frac{1}{2}} \left(1 - \frac{\pi}{3^{1/6}\Gamma^2\left(\frac{1}{3}\right)} \frac{T}{T_c}\right) , \tag{16.89}$$

where

$$T_c = \left(\frac{\beta_t^2 \gamma_t^4 |\tan\phi_s|}{2h\omega_0 \dot{\gamma}_t^2}\right)^{\frac{1}{3}} . \tag{16.90}$$

is the non-adiabatic time. The correction in the second term of Eq. (16.89) is usually small. Thus, the growth in energy spread can be computed easily, and assuming filamentation the growth in emittance can be obtained. This estimate will be valid if T is less than the time to regain stability. The growths for some situations of the Fermilab Main Ring are given in Table 16.4. The corresponding growths obtained from the growth-at-cutoff model are also listed for comparison.

There is at present no reliable simulation of emittance growth. Experimental measurements are also marred by other mechanisms, such as bunch tumbling due to bunch-length mismatch, particles with different momentum crossing transition at different time, etc. Another example at the Fermilab Main Ring is that the bunch emittance usually grows to such a value that scraping occurs. Therefore, it is hard to judge at this moment the reliability of this crude model. On the other hand, this model can certainly be improved to a certain degree by including, for example, the space-charge distortion of the bunch shape, the tilt effect in phase space near transition, as well as the mechanism of overshoot when stability is regained.

Table 16.4: Growth of emittance for the self-bunching and growth-at-cutoff models.

$\dot{\gamma}_t$ (s^{-1})	N_b (10^{10})	Initial Bunch Emittance (eV-s)	Fractional Emittance Growth	
			Self-Bunching Model	Cutoff Model
90	2.2	0.05	4.09	4.06
90	2.2	0.06	3.03	2.43
90	2.2	0.07	2.35	1.83
90	2.2	0.08	1.89	1.54
90	2.2	0.09	1.52	1.38
120	4.0	0.06	5.32	8.16
120	4.0	0.07	4.12	4.17
120	4.0	0.08	3.31	2.78
120	4.0	0.09	2.72	2.14
120	4.0	0.10	2.29	1.80

16.4 EXERCISES

16.1. The Alternating Gradient Synchrotron (AGS) at Brookhaven is a proton ring with a circumference of 807.11 m. The beam crosses transition at $\gamma_t = 8.8$ with $\dot{\gamma}_t = 63\ s^{-1}$. The rf harmonic is $h = 12$ and the synchronous phase is $\phi_s = 27.3°$.
(1) With beam pipe radius 2.356 cm and beam radius 0.5 cm, compute the space-charge impedance at transition and the frequency at which the integrated negative-mass growth is at a maximum.
(2) For a bunch with[‡] 1×10^{12} protons, compute the critical stability parameter c defined in Eq. (16.69) for various bunch areas. Determine the smallest bunch area to avoid negative-mass blowup. Repeat the computation with the intensity of 3×10^{12} protons.

16.2. It is possible that the AGS described in the previous problem is dominated by a broad-band impedance of $Z_0^{\parallel}/n \approx 20\ \Omega$ at 1.5 GHz. Use the simplified model developed in Sec. 16.1.1 to compute the total growth across transition. The bunch area is assumed to be 6 eV-s.

[‡]The AGS is currently running at the intensity of $\sim 1 \times 10^{13}$ particles per bunch with a transition jump. Here, we are estimating the growth without transition jump.

Bibliography

[1] S.Y. Lee and J.M. Wang, *Microwave Instability Across the Transition Energy*, IEEE Trans. Nucl. Sc. **NS-32**, 2323 (1985).

[2] J. Wei, *Longitudinal Dynamics of the Non-Adiabatic Regime on Alternating-Gradient Synchrotrons*, PhD Dissertation, SUNY, Stony Brook, 1990.

[3] K.Y. Ng, *Microwave Stability Limits for the Main Ring and Growth across Transition*, Fermilab Report TM-1383, 1986.

[4] W.W. Lee and L.C. Teng, *Beam-Bunch Length Matching at Transition Crossing*, Proc. 8th Int. Conf. High Energy Accel., Geneva, 1971, p.327.

[5] P. Lucas and J. MacLachlan, *Simulation of Space Charge Effects and Transition Crossing in the Fermilab Booster,* Proc. 1987 IEEE Part. Accel. Conf., Washington, D.C., 1987, p.1114.

[6] W. Hardt, *Gamma-Transition-Jump Scheme of the CPS*, Proc. 9th Int. Conf. High Energy Accel., SLAC, Stanford, 1974, p.434.

[7] E. Keil and B. Zotter, Particle Accelerators **3**, 11 (1972).

[8] I. Kourbanis and K.Y. Ng, *Transition Crossing in the Fermilab Main Ring, Past and Present*, Proc. 1993 IEEE Part. Accel. Conf., Washington, D.C., 1993, p.3630.

[9] J.A. MacLachlan, *ESME: Longitudinal Phase-Space Particle Tracking—Program Documentation*, Fermilab Internal Report TM-1274, 1984.

[10] I. Kourbanis and K.Y. Ng, unpublished.

[11] See for example Ref. 3 or I. Kourbanis and K.Y. Ng, *Main Ring Transition Crossing Simulations,* Proc. Fermilab III Instabilities Workshop, Fermilab, Batavia, U.S., Ed. S. Peggs and M. Harvey, 1990, p.151.

[12] A. Sørenssen, *What Happens Right After Phase Transition?* CERN/MPS/DL 72-14, 1972.

[13] J.M. Hammersley and D.C. Handscomb, *Monte Carlo Methods*, Wiley, 1964.

[14] E. Keil and W. Schnell, CERN Internal Report ISR-TH-RF/69-48, 1969.